Title

Non-Gaussian Diffusion Imaging Shows Brain Myelin and Axonal Changes in Obstructive Sleep Apnea.

Journal

Journal of computer assisted tomography, 41(2)

ISSN

0363-8715

Authors

Tummala, Sudhakar
Roy, Bhaswati
Vig, Ruchi
et al.

Publication Date

2017-03-01

DOI

10.1097/rct.0000000000000537

Peer reviewed

HHS Public Access

Author manuscript

J Comput Assist Tomogr. Author manuscript; available in PMC 2018 March 01.

Published in final edited form as:

J Comput Assist Tomogr. 2017 ; 41(2): 181–189. doi:10.1097/RCT.0000000000000537.

Non-Gaussian Diffusion Imaging Shows Brain Myelin and Axonal Changes in Obstructive Sleep Apnea

Sudhakar Tummala, PhD[1,*], **Bhaswati Roy, PhD**[2,*], **Ruchi Vig, BS**[1], **Bumhee Park, PhD**[1], **Daniel W. Kang, MD**[3], **Mary A. Woo, RN, PhD**[2], **Ravi Aysola, MD**[4], **Ronald M. Harper, PhD**[5,6], and **Rajesh Kumar, PhD**[1,6,7,8,†]

[1]Department of Anesthesiology, University of California at Los Angeles, Los Angeles, CA 90095, USA

[2]UCLA School of Nursing, University of California at Los Angeles, Los Angeles, CA 90095, USA

[3]Department of Medicine, University of California at Los Angeles, Los Angeles, CA 90095, USA

[4]Department of Pulmonary Medicine and Critical Care, University of California at Los Angeles, Los Angeles, CA 90095, USA

[5]Department of Neurobiology, University of California at Los Angeles, Los Angeles, CA 90095, USA

[6]Brain Research Institute, University of California at Los Angeles, Los Angeles, CA 90095, USA

[7]Department of Radiological Sciences, University of California at Los Angeles, Los Angeles, CA 90095, USA

[8]Department of Bioengineering, University of California at Los Angeles, Los Angeles, CA 90095, USA

Abstract

Objective—Obstructive sleep apnea (OSA) is accompanied by brain changes in areas that regulate autonomic, cognitive, and mood functions, which were initially examined by Gaussian-based diffusion tensor imaging measures, but can be better assessed with non-Gaussian measures. We aimed to evaluate axonal and myelin changes in OSA using axial (AK) and radial kurtosis (RK) measures.

Materials and Methods—We acquired DKI data from 22 OSA and 26 controls; AK and RK maps were calculated, normalized, smoothed, and compared between groups using ANCOVA.

Results—Increased AK, indicating axonal changes, emerged in the insula, hippocampus, amygdala, dorsolateral-pons, and cerebellar peduncles, and showed more axonal injury over previously-identified damage. Higher RK, showing myelin changes, appeared in the hippocampus,

[†]**Address for Correspondence:** Rajesh Kumar, PhD, Department of Anesthesiology, David Geffen School of Medicine at UCLA, 56-141 CHS, 10833 Le Conte Ave, University of California at Los Angeles, Los Angeles, CA 90095-1763, USA, Tel: 310-206-6133; 310-206-1679, Fax: 310-825-2236, rkumar@mednet.ucla.edu.

[*]Both authors have equal contribution

Conflicts of interest: None

amygdala, temporal and frontal lobes, insula, midline-pons, and cerebellar peduncles, and showed more wide-spread myelin damage over previously-identified injury.

Conclusion—AK and RK measures showed wide-spread changes over Gaussian-based techniques, suggesting more-sensitive nature of kurtoses to injury.

Keywords

Acute injury; Axial Kurtosis; Radial Kurtosis; Autonomic; Cognition

INTRODUCTION

Obstructive sleep apnea (OSA) is a condition characterized by persistent episodes of complete or partial upper airway obstruction, with continued diaphragmatic efforts to breathe during sleep, leading to intermittent O_2 desaturations.[1,2] Diffusion tensor imaging (DTI) shows that OSA is accompanied by axonal and myelin injury in wide-spread brain areas, including the medulla, cerebellum, basal-ganglia, frontal, and limbic areas that control autonomic, mood and cognitive functions.[3] Variations in the DTI measure can show separately, characteristics of axonal changes vs properties of myelin surrounding in those axons, allowing insight into the nature of mechanisms inducing injury. To assess axonal integrity, DTI-based “axial diffusivity” measures are used; this method measures water diffusion parallel to fibers, with water motion principally constrained by axons to move only parallel to fibers. Water diffusion perpendicular to axons can also be quantified to provide indications of myelin integrity, since defects in myelin integrity will alter water movement through the normally-blocking lipid myelin. Both axial and radial diffusivity measures have been used successfully to track normal developmental changes in brain tissue,[4] as well as changes in myelin and axons in sleep-disordered breathing and heart failure conditions.[3,5]

A major drawback of classic DTI-based procedures is the assumption that displacement of water molecules in the brain follows a Gaussian distribution, a notion that is inappropriate in several circumstances. Water diffusion in biological tissues follows non-Gaussian distribution, due to anisotropic nature of cellular and fiber microstructure, especially in the brain where water diffusion is strongly restricted by crossing fibers and myelinated axons. Numerous circumstances in the brain preclude the possibility of Gaussian distribution for water diffusion; these include the presence of intra-voxel fiber crossing, conditions surround myelinated axons, and complex micro structures.[6,7]

Diffusion kurtosis imaging (DKI), an extension of DTI, is a technique that can characterize non-Gaussian water diffusion within tissue by estimating kurtosis (i.e., the extent of peakedness, suggesting acute changes, or flatness of the displacement distribution, indicating chronic changes).[6] DKI-based axial and radial kurtosis measures, which are directional kurtoses in the direction of, and perpendicular, to axons, could indicate more-precise axonal changes and myelin alternations in the brain, respectively.[3,8] Non-Gaussian DKI measures have shown promising findings in several pathological conditions, including tumor characterization,[9] human brain aging,[10] brain maturation,[11] traumatic brain injury,[12] psychiatric disorders,[13] white matter changes cerebral infarctions,[14] and stroke.[8] Thus, DKI-

based axial and radial kurtosis measures could be useful to characterize axonal and myelin changes more-precisely across the whole-brain in OSA subjects.

Our aim was to investigate regional brain axonal and myelin changes in recently-diagnosed treatment-naïve OSA subjects using DKI-based axial and radial kurtosis measures. We hypothesized that regional axial and radial kurtosis values will be higher in OSA subjects in various brain sites involved in autonomic, respiratory, and neuropsychologic regulation compared to control subjects.

MATERIALS AND METHODS

Design

We used a comparative cross-sectional study design to examine detailed brain axonal and myelin changes in recently-diagnosed, treatment-naïve OSA over control subjects.

Subjects

The study population consisted of 22 new-diagnosed, treatment-naïve OSA and 26 age- and gender-comparable control subjects. Demographic, sleep, clinical, cognitive, and neuropsychologic variables are summarized in Table 1. A subset of OSA and control subjects used here were part of previously-published data examining different research questions.[15,16] All control subjects were without any medication that might change brain tissue, were compatible with the MRI scanner environment (i.e., no metallic implants or iron-based tattoos, and body weights within limits of the scanner), and were recruited through the University of California at Los Angeles (UCLA) campus and West Los Angeles Area. OSA subjects were recruited from the Sleep Disorders Laboratory at the UCLA Medical Center, newly-diagnosed via overnight polysomnography with at least moderate severity (apnea-hypopnea-index ≥ 15; i.e 15 or more apneas or hypopneas were recorded per hour of sleep) and were treatment-naïve for the breathing issue. All OSA subjects were without any cardiovascular-altering medications, such as β-blockers, α-agonists, angiotension-converting enzyme inhibitors and vasodilators, or mood modifying drugs, such as serotonin reuptake inhibitors. All OSA and control subjects with a history of stroke, heart failure, diagnosed brain conditions, metallic implants, were excluded from the study. Both OSA and control subjects provided written informed consent prior to the study, all data collection procedures were carried out in accordance with the Institutional Review Board at UCLA approval.

Assessment of Sleep Quality and Daytime Sleepiness

Two self-administered questionnaires were employed to investigate sleep quality and daytime sleepiness.[17] For all OSA and control subjects, sleep quality was evaluated based on the Pittsburgh sleep quality index (PSQI), a self-rated questionnaire that assess quality of sleep and disturbance over a month, and day time sleepiness, a self-reported questionnaire that shows daytime sleepiness, was examined based on the Epworth sleepiness scale (ESS).

Evaluation of Neuropsychologic Functions

We used the Beck anxiety inventory (BAI) and Beck depression inventory II (BDI-II) self-reported questionnaires with 21 multiple-choice questions for assessment of severity of anxiety and depressive symptoms in OSA and control subjects.[18,19] Both tools are self-administered questionnaires (21 questions; each score ranged from 0–3), with each score ranging from 0–63 based on severity of the symptoms.

Cognition Assessment

For cognitive assessment in OSA and control subjects, we performed the Montreal Cognitive Assessment (MoCA) test, which is designed for fast screening of various cognitive domains, including attention and concentration, executive functions, language, memory, visuo-constructional skills, conceptual thinking, calculations, and orientation. We also conducted the Trial making A & B tests, which are used for screening of dementia, including executive function, visual search, mental flexibility, scanning and speed of processing, to examine the cognitive aspects of OSA and control subjects. Higher MoCA score indicates higher cognition and lower values of Trial making A & B tests indicate no issues with cognitive aspects.

Magnetic Resonance Imaging

Brain images from OSA and control subjects were acquired using a 3.0-Tesla MRI scanner (Magnetom Tim-Trio; Siemens, Erlangen, Germany). Diffusion kurtosis imaging data were collected using echo planar imaging with a twice-refocused spin echo pulse sequence (repetition time (TR) = 7000 ms; echo time (TE) = 90 ms; FA = 90°; bandwidth = 2439 Hz/pixel; matrix size = 82×82; FOV = 230×230 mm; slice thickness = 2.8 mm; isotropic resolution = 2.8 mm; 60 slices; no interslice-gap; diffusion directions = 30; b-values = 0, 1000, and 2000 s/mm^2) in the axial plane, and two separate series were collected for subsequent averaging. High resolution T1-weighted scans were acquired with magnetization prepared rapid acquisition gradient echo sequence in the sagittal plane (repetition time TR = 2200 ms; echo time TE = 2.34 ms; inversion-time = 900 ms; flip-angle = 9°; matrix size = 320×320; field of view (FOV) = 230×230 mm; slice thickness = 0.9 mm). Proton density and T2-weighted images were collected using a dual-echo turbo spin-echo pulse sequence in the axial plane (TR = 10,000 ms; TE1,2 = 17,134 ms; FA = 130°; matrix size = 256×256; FOV = 230×230 mm; slice thickness = 3.5 mm).

Data Processing and Analysis

We used various software for image visualization, data pre-processing, and analyses that included the statistical parametric mapping package SPM8 (Wellcome Department of Cognitive Neurology, UK; http://www.fil.ion.ucl.ac.uk/spm), Diffusional Kurtosis Estimator (DKE),[20] MRIcroN,[21] and MATLAB-based custom routines (The MathWorks Inc, Natick, MA). For all OSA and control subjects, acquired structural images ((T1-, T2-, and PD-weighted) were examined visually to ensure that no serious anatomical defects are apparent. No subjects included here showed any serious brain pathology on visual examination of structural brain images. DKI data were also inspected visually for any motion or other imaging artifacts to ensure that images were acceptable for further analysis.

Axial and Radial Kurtosis Calculation

Axial and radial kurtosis maps were derived from non-diffusion (b = 0 s/mm^2) and diffusion-weighted images (b = 1000 and 2000 s/mm^2). We created a 4-dimensional matrix from non-diffusion and diffusion-weighted images (b = 0, 1000 and 2000 s/mm^2), and this matrix was used for estimation of axial and radial kurtosis maps using DKE software.

Normalization and Smoothing of Axial and Radial Kurtosis Maps

Both axial and radial kurtosis maps, derived from each series, and non-diffusion-weighted (b0) were realigned to remove any possible motion artifacts, and then averaged. Using averaged b0 images of individual subjects, gray matter, white matter, and cerebrospinal fluid (CSF) were partitioned, based on a *priori-defined* distributions of tissue types,[22] and the resulting normalization parameters were applied to the corresponding axial and radial kurtosis maps and b0 images. The normalized axial and radial kurtosis maps were smoothed, using an isotropic Gaussian filter (kernel size, 10 mm).

Background Images

We segmented high-resolution T1-weighted images of a control subject into gray, white, and CSF tissue types, based on *a priori*-defined distributions of gray, white, and CSF using unified segmentation procedure.[22] The normalization parameters, resulting from the segmentation step, were applied to corresponding T1-weighted images. The normalized T1-weighted images were used as background images for structural identification.

Global Brain Mask

We averaged the normalized white matter probability maps, derived from averaged b0 images, from all subjects to create a mean global white matter probability map, and the normalized gray matter probability maps to create a global gray matter probability map. The global white and gray matter probability maps were thresholded (white matter > 0.3; gray matter > 0.3) and combined to create a global brain mask.

Region-of-Interest (ROI) Analyses

We conducted ROI analyses to evaluate magnitude of mean axial and radial kurtosis values in those sites that showed significant differences between OSA and healthy subjects based on voxel-by-voxel analyses. The clusters determined by voxel-by-voxel analyses were used to outline ROIs that were used to calculate average axial and radial kurtosis values with the corresponding smoothed maps.

Statistical Analyses

We used the SPM8 and the IBM statistical package for social sciences (SPSS v22) for statistical analyses. We used independent-samples t-tests and Chi-square test to examine demographic, sleep, neuropsychologic, and cognitive data.

The normalized and smoothed axial and radial kurtosis maps were compared voxel-by-voxel between two groups using analysis of covariance (ANCOVA), with age and gender as covariates (SPM8, uncorrected threshold, $p < 0.005$; no cluster level threshold). Brain

regions with significant differences between groups were overlaid onto background images for structural identification.

The mean axial and radial kurtosis values, derived from ROI analyses, were compared between groups using ANCOVA, with age and gender as covariates. A p value less than 0.05 was considered statistically significant.

RESULTS

Demographics

No significant differences in age ($p = 0.16$) or gender ($p = 0.29$) emerged between OSA and control subjects (Table 1). However, OSA showed higher body mass index compared to control subjects ($p < 0.0001$; Table 1).

Differences in Biophysical, Sleep, Neuropsychological, and Cognitive variables

The PSQI and ESS values were significantly higher in OSA compared to controls (PSQI, $p = 0.0001$; ESS, $p = 0.0003$). Neuropsychological variables showed higher values in OSA than controls, and demonstrated borderline significance levels (BDI-II, $p = 0.045$; BAI, $p = 0.08$). OSA subjects performed significantly worse than control subjects in the MoCA test ($p = 0.03$). No significant differences in heart rate and Trial A & B tests appeared between groups (Table 1).

Axial and Radial Kurtosis changes

Several brain sites showed increased axial and radial kurtosis values in OSA compared to control subjects, with age- and gender-related variables controlled (Fig. 1A, B). Brain sites with increased axial kurtosis appeared in the bilateral mid-to-posterior insular cortices, extending to the external capsule (Fig. 2k, 2l), bilateral hippocampus extending to the amygdala (Fig. 2i, 2j), bilateral ventral and mid temporal white matter (Fig. 2g, 2h), left internal capsule, extending to the caudate (Fig. 2p), left internal capsule extending to the thalamus (Fig. 2m), right occipital cortex (Fig. 2n, 2t), right parietal white matter (Fig. 2c, 2o), right mid corona radiata (Fig. 2d), unilateral dorsolateral pons (Fig. 2f), right middle cerebellar peduncle (Fig. 2a), and lateral parietal white matter extending from lateral cortex to midline (Fig. 2s).

The brain sites with increased radial kurtosis included the bilateral posterior insular cortices, extending to the external capsule and ventral putamen (Fig. 3l, 3m), parietal cortex (Fig. 3f, 3n), bilateral hippocampus, extending to the amygdala (Fig. 3h, 3i), cerebellar vermis (Fig. 3j), right ventral frontal orbital cortex (Fig. 3e), ventral, mid and dorsal temporal cortex, extending to temporal white matter (Fig. 3b), midline pons, extending to the middle cerebellar peduncle (Fig 3a), mid temporal white matter, extending to the hippocampus (Fig. 3c, 3d). No brain regions showed decreased axial and radial kurtosis values in OSA over control subjects.

The insular cortices and surrounding white matter, dorsolateral pons, parietal, and cerebellar areas showed more axonal injury over previously-identified damage with axial diffusivity. Wide-spread myelin injury was also present in insular, external capsule, amygdala, temporal,

midline pons and inferior frontal-orbital areas over already-detected changes with radial diffusivity.

ROI Analyses

The calculated regional axial and radial kurtosis values from various brain sites for both groups are summarized in Table 2 and Table 3, respectively. The regional mean axial and radial kurtosis values are significantly increased in OSA compared to control subjects, consistent with the voxel-by-voxel analyses results.

DISCUSSION

Overview

Clinical variables, including sleep, cognitive, and neuropsychological values differed significantly between newly-diagnosed, treatment-naïve OSA and control subjects. Based on voxel-level analyses, OSA subjects showed significantly increased regional axial and radial kurtosis values, plausibly indicating acute axonal and myelin tissue changes, respectively.[8] Damage appeared in several brain sites essential for autonomic, cognitive, neuropsychological, motor, and respiratory functions, including changes in limbic, basal-ganglia, hippocampus, temporal, parietal, frontal, occipital, pons, and cerebellar sites. More wide-spread changes appear based on DKI measures over DTI,[3] indicating that axial and radial kurtosis measures may be more sensitive tissue markers for acute condition. Our similar OSA patients studied before have shown decreased mean,[23] axial and radial[3] diffusivities, indicating acute tissue damage in the condition. The underlying mechanisms contributing to axonal and myelin injury may include combination of hypoxic, hypercarbic, and perfusion issues accompanying the syndrome.

Brain Tissue Injury in OSA

During obstructive events in OSA subjects, hypoxic/ischemic processes may reduce oxygen supply to the brain tissue, which may trigger water movement from extracellular to intracellular spaces, leading to neuronal and axonal swelling. Axonal and myelin changes, gray matter volume alterations, and metabolic deficits, examined by various MRI and spectroscopy procedures, appear in OSA subjects in multiple areas. Axonal changes in newly-diagnosed OSA subjects, examined by Gaussian diffusion-based axial diffusivity, emerged in the corona radiata, frontal and temporal white matter, limbic sites, corpus callosum, and ventral medulla, and myelin injuries, based on radial diffusivity measures, appeared in the medulla, limbic, cingulum bundle, temporal, and occipital white matter sites.[3,24] However, we now extend the axonal and myelin assessment with kurtosis metrics, which have the potential to provide more precise insights into types of tissue damage.

Diffusivity vs. Kurtosis in Assessment of Axonal and Myelin Injury

Axial and radial kurtosis measures are based on non-Gaussian diffusion phenomena, and therefore, represent markers of diffusional heterogeneity. Tissue heterogeneity decreases in chronic disease conditions due to loss of axons and myelin, neurons, glial cells, synapses and dendrites over the time, and increase of extracellular spaces,[25,26] and increases in acute conditions with axonal and myelin swelling and more tissue organization.[3,5] The probable

mechanism for decreased axial and radial kurtosis is the degeneration of axons and myelin sheath, resulting in increased extracellular fluid, leading to higher degree of water permeability along parallel and perpendicular directions to axons. Thus, kurtosis measures are suitable to differentiate chronic from acute tissue pathology. Previous studies, based on Gaussian diffusion measures, showed reduced axial and radial diffusivity values, indicating that evaluating tissue changes as soon as OSA is diagnosed are still in the acute stage of axonal and myelin pathology.[3] That finding is of significant interest, since interventions to restore tissue integrity are more effective in acute stages.[27] We identified multiple brain regions with increased axial and radial kurtosis values, plausibly due to presence of acute disease condition.[8] In addition, various brain areas, including the insular cortices, internal capsule, middle cerebellar peduncles, parietal white matter, and amygdala showed more wide-spread damage than previously-identified axonal changes. Similarly, wide-spread myelin damage emerged in insular, midline pons, cerebellar vermis, and frontal-orbital sites, not previously-identified on radial diffusivity. The data suggest that kurtosis based measures are more sensitive to the acute disease condition than standard diffusivity based indices.

Axonal and Myelin Changes: Autonomic and Respiratory Control Sites

Significantly increased axial and radial kurtosis values appeared in brain sites responsible for regulation of autonomic and respiratory functions. The insular cortices, midline pons, cerebellar peduncles and cerebellar vermis, regions important for sympathetic outflow, regulation of blood pressure, respiration, and integration of baroreceptor afferents showed more injury.[3,23,28] Abnormal kurtosis in the respiratory control sites plausibly suggests that either incidence of sleep-disordered breathing triggered brain to correct the dysfunction, and the underlying process resulted in neural injury, or the neural damage at specific brain tissue site was responsible for the condition. The axonal and myelin changes in bilateral insular regions, areas that control sympathetic and parasympathetic nervous systems, showed wide spread injury, compared to previously-identified damage. The injury in the right insula could lead to impaired modulation of sympathetic output via either direct, or indirect inputs to the sympathetic preganglionic neurons in spinal cord.[29] Moreover, damage in the midline pons, cerebellar peduncles, and cerebellar vermis, pathways responsible for respiratory and autonomic functions, showed more injury,[30,31] indicating a potential for more marked autonomic and respiratory regulatory consequences.

Axonal and Myelin Changes: Neuropsychologic, Motor, and Cognitive Regulatory Areas

Axonal and myelin changes appeared in sites important for neuropsychologic, motor, and cognitive control. These areas included the hippocampus, amygdala, internal and external capsules, ventral putamen, frontal, parietal, temporal white matter regions. The bilateral ventral putamen showed injury, indicating a potential for compromised motor integration and coordination in OSA.[32] The injury in internal and external capsules may interfere with sensory and motor integration, as well as signaling necessary for neuropsychologic functions, including mood and anxiety symptoms, since damage may interrupt projections from adjacent white matter tracts and the basal-ganglia.[33] Along with autonomic deficits, insular injury may also interfere with regulation of emotions, an especially important aspect with OSA, which has a very high incidence of depression and anxiety symptoms, demonstrated in the findings here, as well as by earlier studies.[34,35] Myelin changes in the

ventral fronto-orbital cortex could contribute to cognitive processes, as well as blood pressure regulation.[36,37] Axonal injury found in the occipital cortex may influence visual processing in OSA subjects.[38] Moreover, the axonal and myelin changes in bilateral parietal, temporal, and hippocampal regions may contribute to deficits in speech and object processing, cognitive regulation, and long-term memory retrieval, functions that are deficient in the condition.[39,40]

Limitations

Although statistically significant results emerged with a relatively small number of OSA subjects, indicating large effect sizes between groups, the clinical relevance of these findings would be enhanced with a larger study population. Although we targeted to recruit newly-diagnosed, treatment-naïve OSA subjects, the precise OSA disease durations were unknown, since multiple factors can contribute to variable delays in diagnosis. However, our results show increased regional axial and radial kurtosis values, indicating that a majority of the OSA subjects were in acute stages of brain pathology. Significant differences emerged in systolic blood pressure and body-mass-index between groups and some of the findings might be due to differences in these variables.[41,42]

Conclusions

Evaluation of regional brain areas of newly-diagnosed, treatment-naïve OSA patients with diffusion kurtosis imaging showed increased axial and radial kurtosis values, suggesting that changes in axons and myelin were probably in acute stages. These axonal and myelin changes appeared in several brain sites essential for autonomic, motor, respiratory, mood, and cognitive regulation, and included limbic, basal-ganglia, hippocampal, temporal, parietal, frontal, pontine, and cerebellar sites. Axonal changes in OSA were more wide-spread than myelin deficits. Recurrent hypoxic, hypercarbic, perfusion, and arousal processes accompanying apnea and recovery from apnea in OSA may contribute to axonal and myelin pathology. The findings indicate that axial and radial kurtosis indices may be more sensitive measures to evaluate axonal and myelin integrity, and assist in assessment of brain sites that play significant roles in mediating deficits in OSA subjects.

Acknowledgments

Grant Support: This research work was supported by National Institutes of Health R01 HL-113251 and R01 NR-015038.

We thank Mrs. Karen A. Harada and Ms. Kelly A. Hickey for assistance with data collection.

Abbreviations

OSA	Obstructive Sleep Apnea
DTI	Diffusion Tensor Imaging
DKI	Diffusion Kurtosis Imaging
PSQI	Pittsburgh Sleep Quality Index

ESS	Epworth Sleepiness Scale
BAI	Beck Anxiety Inventory
BDI-II	Beck Depression Inventory II
MoCA	Montreal Cognitive Assessment
DKE	Diffusional Kurtosis Estimator
ANCOVA	Analysis of Covariance

REFERENCES

1. Patil SP, Schneider H, Schwartz AR, et al. Adult obstructive sleep apnea: pathophysiology and diagnosis. Chest. 2007; 132:325–337. [PubMed: 17625094]
2. Lurie A. Obstructive sleep apnea in adults: epidemiology, clinical presentation, and treatment options. Adv Cardiol. 2011; 46:1–42. [PubMed: 22005188]
3. Kumar R, Pham TT, Macey PM, et al. Abnormal myelin and axonal integrity in recently diagnosed patients with obstructive sleep apnea. Sleep. 2014; 37:723–732. [PubMed: 24899761]
4. Sullivan EV, Rohlfing T, Pfefferbaum A. Longitudinal study of callosal microstructure in the normal adult aging brain using quantitative DTI fiber tracking. Dev Neuropsychol. 2010; 35:233–256. [PubMed: 20446131]
5. Kumar R, Woo MA, Macey PM, et al. Brain axonal and myelin evaluation in heart failure. J Neurol. Sci. 2011; 307:106–113. [PubMed: 21612797]
6. Jensen JH, Helpern JA. MRI quantification of non-Gaussian water diffusion by kurtosis analysis. NMR Biomed. 2010; 23:698–710. [PubMed: 20632416]
7. Hagmann P, Jonasson L, Maeder P, et al. Understanding diffusion MR imaging techniques: from scalar diffusion-weighted imaging to diffusion tensor imaging and beyond. Radiographics. 2006; 26(Suppl 1):S205–S223. [PubMed: 17050517]
8. Hui ES, Fieremans E, Jensen JH, et al. Stroke assessment with diffusional kurtosis imaging. Stroke. 2012; 43:2968–2973. [PubMed: 22933581]
9. Van Cauter S, Veraart J, Sijbers J, et al. Gliomas: diffusion kurtosis MR imaging in grading. Radiology. 2012; 263:492–501. [PubMed: 22403168]
10. Gong NJ, Wong CS, Chan CC, et al. Aging in deep gray matter and white matter revealed by diffusional kurtosis imaging. Neurobiol Aging. 2014; 35:2203–2216. [PubMed: 24910392]
11. Cheung MM, Hui ES, Chan KC, et al. Does diffusion kurtosis imaging lead to better neural tissue characterization? A rodent brain maturation study. Neuroimage. 2009; 45:386–392. [PubMed: 19150655]
12. Stokum JA, Sours C, Zhuo J, et al. A longitudinal evaluation of diffusion kurtosis imaging in patients with mild traumatic brain injury. Brain. Inj. 2014:1–11.
13. Delgado y Palacios R, Verhoye M, Henningsen K, et al. Diffusion kurtosis imaging and high-resolution MRI demonstrate structural aberrations of caudate putamen and amygdala after chronic mild stress. PLoS. One. 2014; 9:e95077. [PubMed: 24740310]
14. Taoka T, Fujioka M, Sakamoto M, et al. Time course of axial and radial diffusion kurtosis of white matter infarctions: period of pseudonormalization. AJNR Am J Neuroradiol. 2014; 35:1509–1514. [PubMed: 24699091]
15. Park BPJ, Woo MA, Kang DW, Macey PM, Yan-Go FL, Harper RM, Kumar R. Aberrant Insular Functional Network Integrity in Patients with Obstructive Sleep Apnea. SLEEP. 2016
16. Tummala S, Palomares J, Kang DW, et al. Global and Regional Brain Non-Gaussian Diffusion Changes in Newly Diagnosed Patients With Obstructive Sleep Apnea. Sleep. 2015
17. Knutson KL, Rathouz PJ, Yan LL, et al. Stability of the Pittsburgh Sleep Quality Index and the Epworth Sleepiness Questionnaires over 1 year in early middle-aged adults: the CARDIA study. Sleep. 2006; 29:1503–1506. [PubMed: 17162998]

18. Beck AT, Epstein N, Brown G, et al. An inventory for measuring clinical anxiety: psychometric properties. J Consult Clin Psychol. 1988; 56:893–897. [PubMed: 3204199]
19. Beck AT, Steer RA, Ball R, et al. Comparison of Beck Depression Inventories -IA and -II in psychiatric outpatients. J Pers Assess. 1996; 67:588–597. [PubMed: 8991972]
20. Tabesh A, Jensen JH, Ardekani BA, et al. Estimation of tensors and tensor-derived measures in diffusional kurtosis imaging. Magn Reson. Med. 2011; 65:823–836. [PubMed: 21337412]
21. Rorden C, Karnath HO, Bonilha L. Improving lesion-symptom mapping. J Cogn Neurosci. 2007; 19:1081–1088. [PubMed: 17583985]
22. Ashburner J, Friston KJ. Unified segmentation. Neuroimage. 2005; 26:839–851. [PubMed: 15955494]
23. Kumar R, Chavez AS, Macey PM, et al. Altered global and regional brain mean diffusivity in patients with obstructive sleep apnea. J Neurosci. Res. 2012; 90:2043–2052. [PubMed: 22715089]
24. Kumar R, Nguyen HD, Macey PM, et al. Regional brain axial and radial diffusivity changes during development. J Neurosci. Res. 2012; 90:346–355. [PubMed: 21938736]
25. Gong NJ, Wong CS, Chan CC, et al. Correlations between microstructural alterations and severity of cognitive deficiency in Alzheimer's disease and mild cognitive impairment: a diffusional kurtosis imaging study. Magn Reson Imaging. 2013; 31:688–694. [PubMed: 23347602]
26. Kazumata K, Tha KK, Narita H, et al. Characteristics of Diffusional Kurtosis in Chronic Ischemia of Adult Moyamoya Disease: Comparing Diffusional Kurtosis and Diffusion Tensor Imaging. AJNR Am J Neuroradiol. 2016
27. Prabhakaran S, Ruff I, Bernstein RA. Acute stroke intervention: a systematic review. JAMA. 2015; 313:1451–1462. [PubMed: 25871671]
28. Woodson BT, Brusky LT, Saurajen A, et al. Association of autonomic dysfunction and mild obstructive sleep apnea. Otolaryngol Head Neck Surg. 2004; 130:643–648. [PubMed: 15195047]
29. Lundblad LC, Fatouleh RH, Hammam E, et al. Brainstem changes associated with increased muscle sympathetic drive in obstructive sleep apnoea. Neuroimage. 2014; 103C:258–266.
30. Alheid GF, Milsom WK, McCrimmon DR. Pontine influences on breathing: an overview. Respir Physiol Neurobiol. 2004; 143:105–114. [PubMed: 15519548]
31. Holmes MJ, Cotter LA, Arendt HE, et al. Effects of lesions of the caudal cerebellar vermis on cardiovascular regulation in awake cats. Brain. Res. 2002; 938:62–72. [PubMed: 12031536]
32. Kumar R, Farahvar S, Ogren JA, et al. Brain putamen volume changes in newly-diagnosed patients with obstructive sleep apnea. Neuroimage Clin. 2014; 4:383–391. [PubMed: 24567910]
33. Kumar R, Macey PM, Cross RL, et al. Neural alterations associated with anxiety symptoms in obstructive sleep apnea syndrome. Depress Anxiety. 2009; 26:480–491. [PubMed: 18828142]
34. Yadav SK, Kumar R, Macey PM, et al. Insular cortex metabolite changes in obstructive sleep apnea. Sleep. 2014; 37:951–958. [PubMed: 24790274]
35. Macey PM, Kumar R, Woo MA, et al. Brain structural changes in obstructive sleep apnea. Sleep. 2008; 31:967–977. [PubMed: 18652092]
36. Wallis JD. Orbitofrontal cortex and its contribution to decision-making. Annu Rev Neurosci. 2007; 30:31–56. [PubMed: 17417936]
37. Chapman WP, Livingston RB, Livingston KE. Frontal lobotomy and electrical stimulation of orbital surface of frontal lobes; effect on respiration and on blood pressure in man. Arch Neurol Psychiatry. 1949; 62:701–716.
38. Price CJ, Devlin JT. The myth of the visual word form area. Neuroimage. 2003; 19:473–481. [PubMed: 12880781]
39. Holdstock JS. The role of the human medial temporal lobe in object recognition and object discrimination. Q J Exp Psychol B. 2005; 58:326–339. [PubMed: 16194972]
40. Bontempi B, Laurent-Demir C, Destrade C, et al. Time-dependent reorganization of brain circuitry underlying long-term memory storage. Nature. 1999; 400:671–675. [PubMed: 10458162]
41. Kilicarslan R, Alkan A, Sharifov R, et al. The effect of obesity on brain diffusion alteration in patients with obstructive sleep apnea. Scientific World Journal. 2014; 2014:768415. [PubMed: 24729752]

42. Salat DH, Williams VJ, Leritz EC, et al. Inter-individual variation in blood pressure is associated with regional white matter integrity in generally healthy older adults. Neuroimage. 2012; 59:181–192. [PubMed: 21820060]

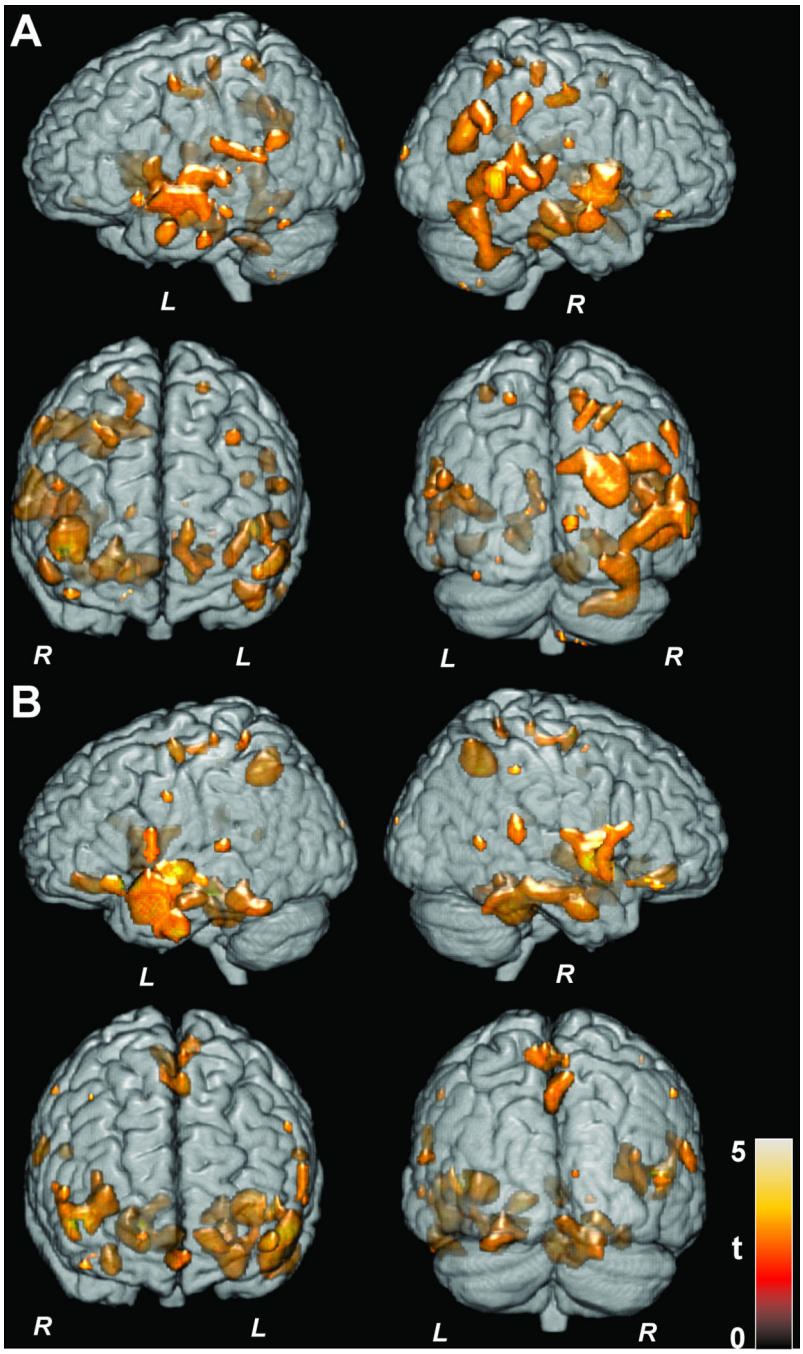

Figure 1. 3D whole-brain demonstrating altered axial and radial kurtosis

Brain sites with significantly increased axial (A) and radial (B) kurtosis values in obstructive sleep apnea compared to control subjects. Sites are overlaid onto a 3D whole-brain cortical surface for anatomical identification, and are shown in different axial, coronal, and sagittal views.

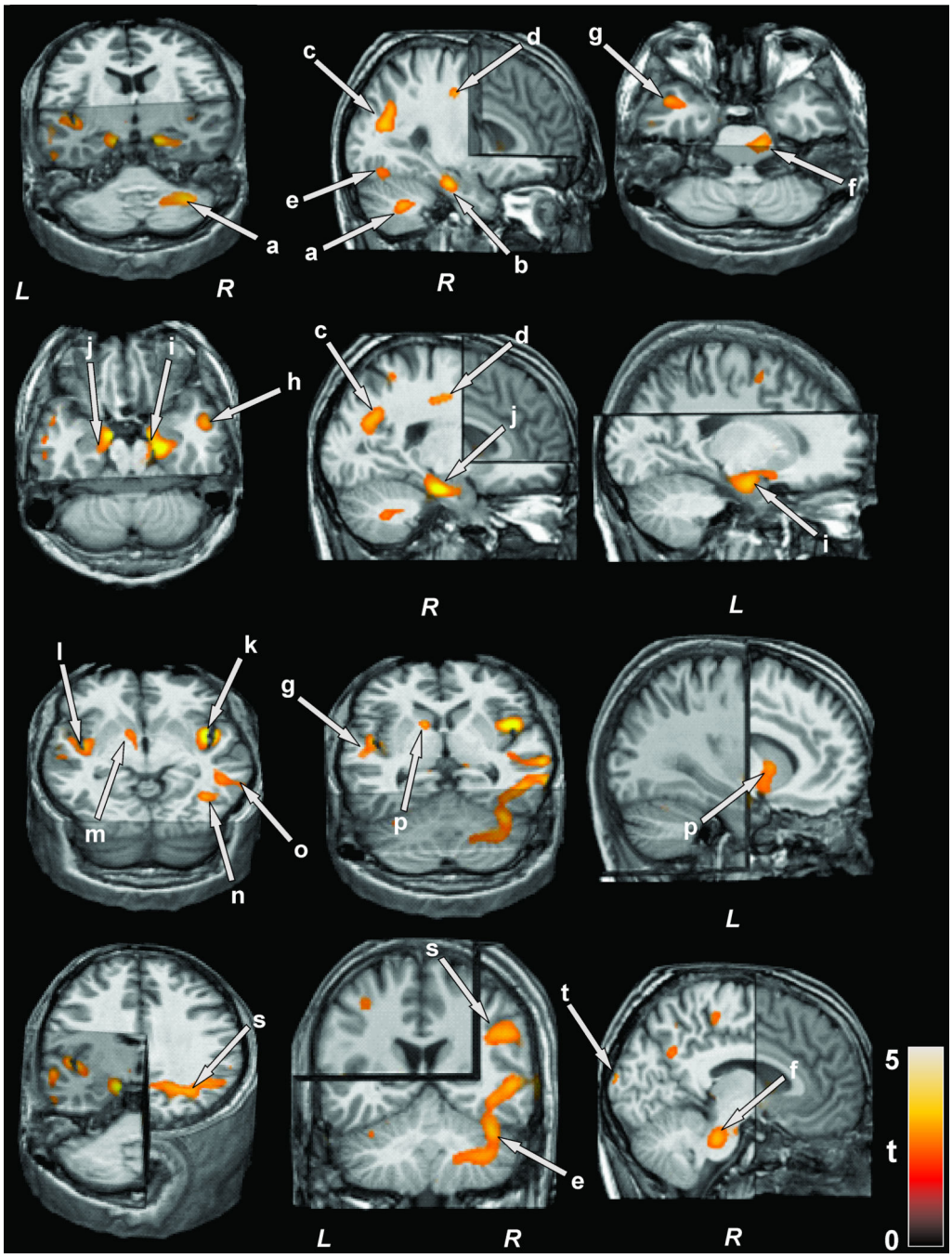

Figure 2. Brain regions showing altered axial kurtosis

3D brain sites showing regions with higher axial kurtosis values in obstructive sleep apnea over control subjects. These sites included the right middle cerebellar peduncle (a), hippocampus (b), parietal white matter (c, o), mid corona radiata (d), ventral temporal cortex extending to cerebellar cortex (e), unilateral dorsolateral pons (f), mid, caudal temporal cortices (g, h), hippocampus extending to amygdala (i, j) mid and posterior insular cortices extending to external capsule and ventral putamen (k, l), left internal capsule extending to the thalamus (m), left internal capsule extending to caudate (p), occipital cortex (n, t), and

lateral parietal cortex extending to midline (s). Images are in neurological convention (L, left; R, right), and color bar represents t-statistic values.

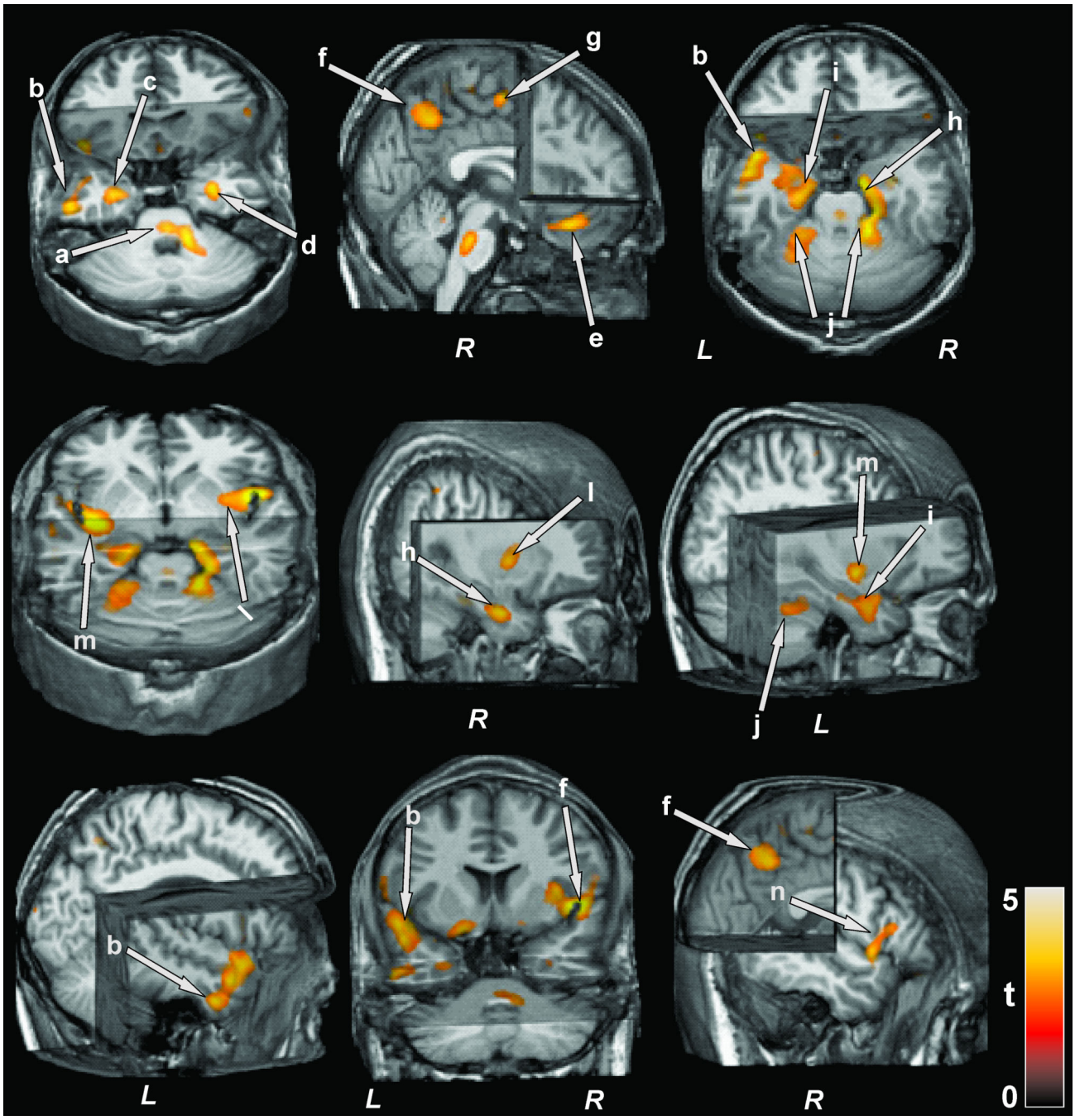

Figure 3. Brain regions showing altered radial kurtosis

3D brain regions with increased radial kurtosis values in obstructive sleep apnea over control subjects. These regions appeared in the midline pons, extending to the middle cerebellar peduncle (a), ventral, mid, dorsal temporal cortex extending to temporal white matter (b), temporal white matter extending to the hippocampus (c, d), inferior frontal orbital cortex (e), parietal cortex (f, n), midline frontal cortex (g), hippocampus extending to amygdala (i, h),

cerebellar vermis (j), insular cortex extending to external capsule and ventral putamen (m, l). Figure conventions are same as in Figure 2.

Table 1

Demographic, physiologic, neuropsychologic, sleep, and cognitive data of control and OSA subjects.

Variables	Control (mean ± SD) N = 26	OSA (mean ± SD) N = 22	P-value
Age (years)	45.6 ± 9.3	49.2 ± 8.4	0.16
Gender	11 female	6 female	0.28
BMI (kg/m^2)	25.4 ± 3.6	32.9 ± 7.9	< 0.0001
Education (years)	17.4 ± 2.9	17.3 ± 3.5	0.97
Heart Rate (beats/min)	74.7 ± 14.5	78.6 ± 12.2	0.35
Systolic BP (mmHg)	115.5±15.8	128.7±15.0	0.008
Diastolic BP (mmHg)	73.7±11.4	79.9±9.7	0.065
MoCA	27.8 ± 2	25.6 ± 4.5	0.03
PSQI	3.6 ± 3	7.8 ± 3.9	0.0001
ESS	3.9 ± 3	7.8 ± 3.9	0.0003
BDI-II	2.7 ± 3.4	5.1 ± 4.6	0.045
BAI	2.5 ± 3.3	4.5 ± 4.5	0.08
Trial A	28.3 ± 8.6	32.8 ± 19	0.28
Trial B	61.6 ± 22.1	68.9 ± 36.5	0.39
AHI (events/hr)	-	43.1±28.3	-

Table legend: BMI: Body Mass Index, BP: Blood Pressure, MoCA: Montreal Cognitive Assessment, PSQI: Pittsburgh Sleep Quality Index, ESS: Epworth Sleepiness Scale, BDI-II: Beck Depression Inventory II, BAI: Beck Anxiety Inventory, AHI: Apnea-Hypopnea-Index, SD: Standard Deviation.

Table 2

Regional mean axial kurtosis values of control and OSA subjects.

Brain region	Control (mean ± SD) N = 26	OSA (mean ± SD) N = 22	Cluster Size (voxels)	P (T)-value (Control vs OSA)
R insular cortex extending to temporal cortex (k)	0.83 ± 0.03	0.88 ± 0.04	1098	< 0.0001 (4.4)
R hippocampus extending to amygdala (i)	0.75 ± 0.03	0.80 ± 0.04	1395	0.0002 (4.0)
L hippocampus extending to amygdala (j)	0.74 ± 0.03	0.79 ± 0.04	981	0.0001 (3.8)
R mid temporal cortex extending to cerebellar peduncles and cortex (a, e)	0.78 ± 0.04	0.83 ± 0.04	4143	< 0.0001 (3.6)
R mid corona radiata (d)	0.70 ± 0.02	0.73 ± 0.03	183	< 0.0001 (3.4)
R lateral parietal cortex extending to midline (s)	0.73 ± 0.04	0.78 ± 0.03	2136	< 0.0001 (3.4)
L insular cortex (l)	0.75 ± 0.02	0.78 ± 0.04	1451	0.001 (3.3)
L mid temporal cortex (g)	0.79 ± 0.04	0.83 ± 0.04	308	0.0005 (3.2)
R superior parietal cortex (c, o)	0.79 ± 0.03	0.82 ± 0.05	164	0.001 (3.2)
L internal capsule extending to caudate (p)	0.90 ± 0.03	0.93 ± 0.03	39	0.0004 (3.2)
R mid temporal cortex (h)	0.74 ± 0.04	0.77 ± 0.03	256	0.0009 (3.2)
L internal capsule extending to thalamus (m)	0.72 ± 0.03	0.76 ± 0.03	313	0.0015 (3.2)
R occipital cortex (n, t)	0.79 ± 0.05	0.84 ± 0.04	153	0.003 (3.2)
R mid dorsolateral pons (f)	0.79 ± 0.04	0.83 ± 0.04	122	0.0002 (3.2)

Table Legend: OSA: obstructive sleep apnea, SD: Standard Deviation, L: Left, R: Right. Brain region labels correspond to Figure 1.

Table 3

Regional mean radial kurtosis values of control and OSA subjects.

Brain region	Control (mean ± SD) N = 26	OSA (mean ± SD) N = 22	Cluster Size (voxels)	P (T)-value (Control vs OSA)
R insular cortex extending to ventral putamen and temporal cortex (l, d)	0.78 ± 0.02	0.83 ± 0.03	1333	< 0.0001 (4.5)
L insular cortex extending to temporal cortex, hippocampus and amygdala (m, b, i, c)	1.07 ± 0.05	1.14 ± 0.06	3852	< 0.0001 (3.9)
R midline pons extending to cerebellar peduncle (a)	0.73 ± 0.02	0.77 ± 0.03	1899	< 0.0001 (3.6)
R hippocampus extending to amygdala (h)	0.66 ± 0.03	0.70 ± 0.03	268	0.0002 (3.6)
R inferior orbital-frontal cortex (e)	0.68 ± 0.02	0.71 ± 0.02	308	0.0006 (3.3)
R parietal cortex (f, n)	0.78 ± 0.04	0.83 ± 0.05	502	0.0004 (3.3)
R midline frontal cortex (g)	0.71 ± 0.05	0.76 ± 0.04	184	0.0004 (3.3)
Cerebellar vermis (j)	0.78 ± 0.02	0.81 ± 0.04	632	0.0009 (3.2)

Table Legend: OSA: obstructive sleep apnea, SD: Standard Deviation, L: Left, R: Right. Brain region labels correspond to Figure 2.